

# Analysis and correction of the magnetic field effects in the Hybrid Photo-Detectors of the RICH2 Ring Imaging Cherenkov detector of LHCb.

**R. Cardinale<sup>a,\*</sup>, C. D'Ambrosio<sup>b</sup>, R. Forty<sup>b</sup>, C. Frei<sup>b</sup>, T. Gys<sup>b</sup>, A. Petrolini<sup>a</sup>, D. Piedigrossi<sup>b</sup>, B. Storaci<sup>b,c,†</sup> and M. Villa<sup>b,c,‡</sup>**

<sup>a</sup>*Dipartimento di Fisica dell'Università di Genova e INFN sezione di Genova, Genova, Italy*

<sup>b</sup>*European Organization for Nuclear Research (CERN), Geneva, Switzerland*

<sup>c</sup>*Dipartimento di Fisica dell'Università di Milano Bicocca e INFN sezione di Milano Bicocca, Milano, Italia.*

*E-mail: roberta.cardinale@ge.infn.it*

**ABSTRACT:** The Ring Imaging Cherenkov detectors of the LHCb experiment at the Large Hadron Collider at CERN are equipped with Hybrid Photo-Detectors. These vacuum photo-detectors are affected by the stray magnetic field of the LHCb magnet, which degrades their imaging properties. This effect increases the error on the Cherenkov angle measurement and would reduce the particle identification capabilities of LHCb. A system has been developed for the RICH2 Ring Imaging Cherenkov detector to perform a detailed characterisation of the magnetic distortion effects. It is described, along with the methods implemented to correct for these effects, restoring the optimal resolution.

**KEYWORDS:** Cherenkov detectors, Photon Detectors for UV, visible and IR photons (vacuum), Detector alignment and calibration methods.

---

\*Corresponding author.

<sup>†</sup>Now at NIKHEF National Institute for Subatomic Physics, Amsterdam, Netherlands

<sup>‡</sup>Now at Physikalisches Institut der Universität Bonn, Bonn, Germany and European Organization for Nuclear Research (CERN), Geneva, Switzerland

---

## Contents

<b>1. Introduction</b>	<b>1</b>
1.1 The LHCb experiment at the LHC	1
1.2 The RICH detectors of LHCb	2
1.3 The HPD of the RICH detectors	3
1.4 The stray magnetic field in RICH2	4
<b>2. Experimental setup</b>	<b>5</b>
2.1 The light projector	5
2.2 The projected light pattern	5
2.3 The pattern alignment procedure	6
<b>3. Data Analysis</b>	<b>6</b>
3.1 Reconstruction Algorithm	7
3.1.1 Noisy pixel masking	7
3.1.2 Ion-feedback reduction	7
<b>4. Correction of the Magnetic Distortions</b>	<b>8</b>
4.1 Parametrisation	9
4.2 Correction procedure	14
<b>5. Correction of the magnetic distortion in the first LHCb data</b>	<b>15</b>
<b>6. Conclusions</b>	<b>15</b>
<b>7. Acknowledgements</b>	<b>16</b>

---

## 1. Introduction

### 1.1 The LHCb experiment at the LHC

The LHCb experiment [1] at the Large Hadron Collider (LHC) [2] at CERN (Geneva, Switzerland) is designed for high precision measurements of CP violation and rare decays of heavy flavours. Key physics measurements to be performed with LHCb are discussed in [3]. A drawing of the LHCb detector is shown in Figure 1.

Particle IDentification (PID) of hadrons is an essential tool for the LHCb physics program. Many final states of interesting decay channels have background from decays with the same topology, but different final state hadrons.

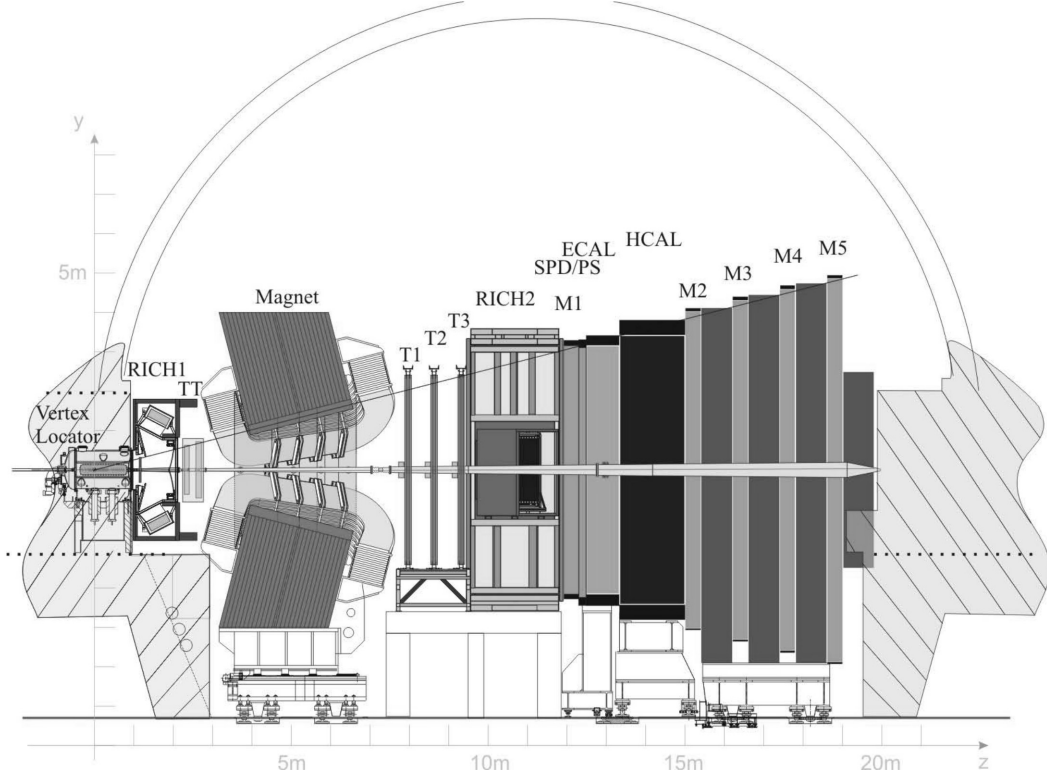


**Figure 1.** A schematic view of the LHCb detector and its subdetectors.

## 1.2 The RICH detectors of LHCb

The PID capabilities of the LHCb apparatus rely on its two Ring Imaging Cherenkov detectors, RICH1 and RICH2 [1, 4].

A single RICH detector cannot satisfy the broad momentum range requirement. However the strong polar angle and momentum correlation can be exploited by a system of two RICHes: RICH1 and RICH2. The two combined sub-detectors can distinguish kaons, pions and protons in the momentum range  $1 \div 100 \text{ GeV}/c$  over the full angular acceptance of LHCb by using three different radiator materials.

The RICH1 detector is located close to the interaction point, upstream of the LHCb magnet, with  $25 - 300 \text{ mrad}$  polar angular acceptance. It employs  $\text{C}_4\text{F}_{10}$  gas and silica aerogel as Cherenkov radiators providing particle identification of low momentum tracks, over the range  $1 - 40 \text{ GeV}/c$ .

The RICH2 detector is located approximately half-way between the LHCb magnet and the large ferromagnetic mass of the muon detector system at a distance along the beam axis of about 6 m from the magnet centre and of about 10 m from the collision point. It is intended for high momentum, up to  $100 \text{ GeV}/c$ , and small polar angle tracks, and uses a gaseous  $\text{CF}_4$  radiator. It covers  $10 - 120 \text{ mrad}$  in the horizontal plane and  $10 - 100 \text{ mrad}$  in the vertical plane.

Both RICH detectors have a similar optical geometry. Cherenkov photons, produced by charged particles traversing the radiator media above the momentum threshold for Cherenkov light production, are focused by spherical mirrors and reflected off flat mirrors onto a photo-sensitive matrix of Hybrid Photo-Detectors (HPD) [1, 5], described in Section 1.3. Each RICH detector has

two HPD planes, above and below the beam pipe for RICH1, on both sides of the beam pipe for RICH2.

The RICH detectors are located in the stray field of the LHCb dipole magnet that has an integrated magnetic field of 4 Tm. The HPDs are affected by the stray magnetic field. As the HPDs must operate with optimal efficiency and imaging performance, it is important to understand, measure and correct for its effects [7]. In this paper the strategy to measure and correct the magnetic distortions in RICH2 are described. Another dedicated system has been developed for RICH1 [8]. A drawing of RICH2 is shown in Figure 2.

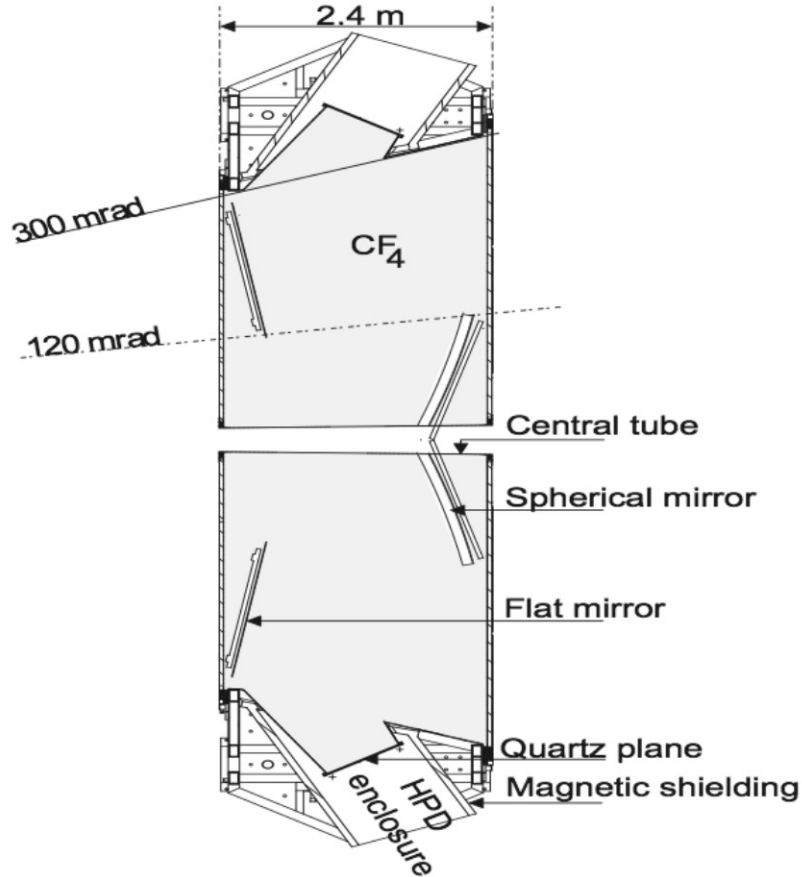


**Figure 2.** A drawing of RICH2 showing the beam pipe, the spherical mirrors, the flat mirrors and the HPD enclosure.

### 1.3 The HPD of the RICH detectors

A schematic view of an HPD [5] is shown in Figure 3.

Photons reaching the HPD photocathode, on the inner-side of the quartz entrance window, produce photoelectrons which are accelerated and focused by the internal electrostatic field inside the vacuum tube. Photoelectrons are detected by a silicon pixel anode chip with 32 columns  $\times$  32 rows of pixels, bump-bonded to a binary electronics readout chip. The photocathode is biased at  $-18$  kV with respect to the anode.

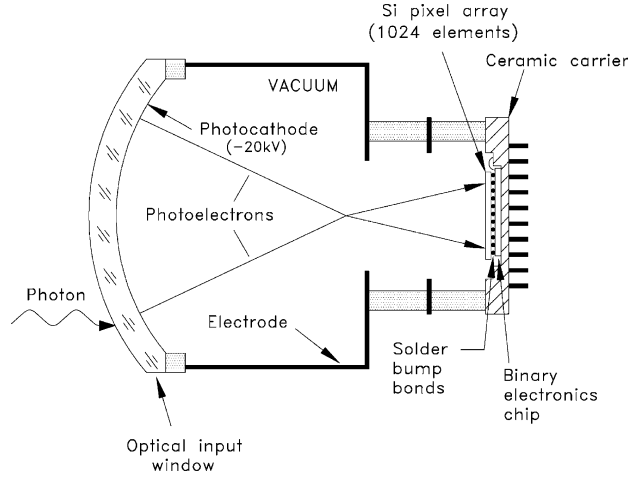


**Figure 3.** A schematic view of the LHCb RICH HPD.

The demagnification produced by the electrostatic field is such that the effective pixel size of  $0.5 \times 0.5 \text{ mm}^2$  on the anode chip corresponds to  $2.5 \times 2.5 \text{ mm}^2$  on the HPD entrance window.

In presence of magnetic field photoelectrons inside the HPD are deviated by the Lorentz force. The imaging properties of the HPD are therefore worsened. If no correction is applied, the error on the Cherenkov angle measurement increases, degrading the PID capability of LHCb.

#### 1.4 The stray magnetic field in RICH2

The effect of the stray magnetic field on the photoelectrons trajectories depends on the intensity and direction of the magnetic field inside the HPD [9]. In a first approximation, when the direction of the magnetic field is perpendicular to the geometrical axis of the HPD, there is an image displacement; on the other hand when the magnetic field is parallel to this axis, photoelectrons move along a spiral trajectory causing a rotation of the image [9].

The stray magnetic field inside RICH2 has been calculated [10] and it reaches up to  $\sim 15 \text{ mT}$  in amplitude with varying directions. In order to reduce its effects on the HPDs, the phototubes matrix has been installed inside a 6 cm thick iron shielding box. Moreover each single HPD is surrounded by a 0.8 mm thick cylindrical shield made of Mu-Metal<sup>®</sup>. This shielding effectively reduces the stray magnetic field inside the HPD. Simulations [11] estimate this residual field to be less than  $\approx 1 \text{ mT}$  with a direction approximately parallel to the HPD geometrical axis and an absolute value dependent on the HPD position within the shielding box.

Measurements have been performed showing that if the field inside the HPD volume is less than  $\approx 1 \text{ mT}$  there is no loss of photoelectrons [12].

However this residual stray magnetic field produces a non-negligible image distortion.

A detailed characterisation procedure of the magnetic distortion effects is necessary to implement a correction. Measurements with magnetic field on and off have been performed, in order to parametrise the effects and to determine a correction procedure restoring the optimal resolution.

## 2. Experimental setup

The correction of the magnetic distortion effect for RICH2 is based on the projection of a known light pattern onto the two  $16 \times 9$  HPD matrices, using a commercial light projector. The pattern is a suitable grid of light spots and its layout can be chosen to optimise the measurements results.

Data with the LHCb magnetic field on and off have been taken and analysed to compare the position of the light spots in the two conditions.

The ultimate goal is to achieve an accuracy in the correction procedure such that the residual uncertainty due to magnetic distortion is negligible, in comparison to the HPD pixel size error [7].

### 2.1 The light projector

A commercial light projector <sup>1</sup> [13] has been used to project the image onto the HPD matrix.

Its most relevant specifications are summarised in Table 1.

**Table 1.** Main specifications of the Samsung SP-P310ME light projector.

Resolution	800 × 600 pixel
Contrast	1000 : 1
Luminosity	50 ANSI Lumen (1300 Lux)
Image size at 2 m distance	101.6 × 76.2 cm <sup>2</sup>
Weight	0.7 Kg
Dimensions (w × h × d)	12.7 cm × 5.1 cm × 9.4 cm

Two such light projectors have been temporarily installed during the LHCb commissioning phase inside the RICH2 gas vessel to shine onto the entire HPD matrix. They were centrally and symmetrically positioned for the two sides, at mid-height and at a distance of  $\sim 3.3$  m from the HPD plane. Neutral filters have been used in order to reduce the number of photons hitting the HPDs, to avoid possible damage of the photocathodes.

The choice of using a light projector, instead of a dedicated light source system, has some advantages. The light projector, thanks to its reduced size, is very easy to handle, transport and install inside RICH2. It does not contribute to the LHCb detector material budget and it is not necessary for it to be radiation hard. Moreover it allows to choose the shape of the projected light pattern with a high spatial resolution.

### 2.2 The projected light pattern

A grid of light spots on a black background has been projected onto the HPD matrix. In order to have the best discrimination for image movements, the smallest possible light spot size was chosen, corresponding to one pixel of the light projector. Since the light projector has been installed at  $\sim 3.3$  m distance from the HPD matrix, the projected size of the pixel is  $2 \times 2$  mm<sup>2</sup> on the photocathode. This size is approximately equal to the RICH2 pixel size and it matches well the optical resolution of the light projector.

The grid is made of single bright pixels separated by five dark pixels (see Figure 4). This is a good compromise to have a large enough number of projected light spots, for better statistics, and

---

<sup>1</sup>Samsung SP-P310ME

the need of a suitable minimum separation between two nearby light spots, to avoid superposition of different light spots during the image reconstruction.

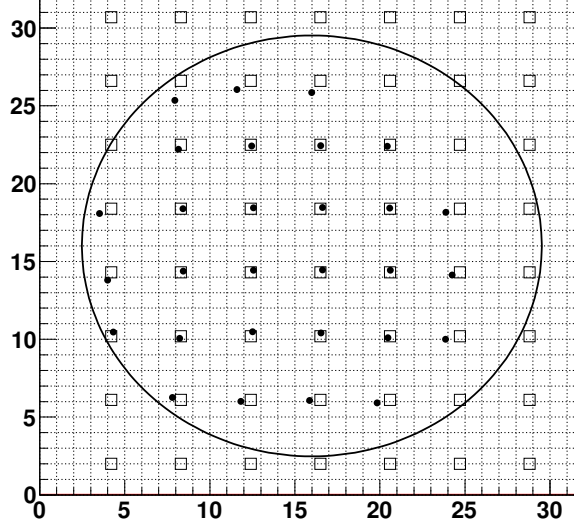


**Figure 4.** One typical HPD chip ( $32 \times 32$  pixels matrix) with the projected pattern (grid of squares) and the reconstructed spots (superimposed dots) affected by refraction effects and reconstruction errors. Points on the HPD right side are not reconstructed because the HPD shielding partially shades the projector light which is not perpendicular with respect to the HPD plane.

The pattern has also three larger spots corresponding to the position of three dedicated PMTs that have been installed in each of the HPD matrix to be used for aligning the pattern.

### 2.3 The pattern alignment procedure

Six Hamamatsu H3164-10 PMTs [14] have been installed inside the HPD matrix, three per side.

These PMTs are used to align the pattern and to know the exact position of the light spots in the LHCb coordinate frame, since the PMT position coordinates are precisely known from the survey of RICH2 [6]. This allows to check that the pattern position is always the same over time.

In order to align the pattern, the image is moved until a maximum in the signal coming from the three alignment PMTs is found. In this way one can reconstruct the pattern position in the global coordinate system and the global position of each HPD is known.

The data acquisition system for the alignment PMTs is described in [15].

## 3. Data Analysis

An algorithm to reconstruct the position of the light spots has been implemented. It can be used both to reconstruct the pattern with and without magnetic field and for internal alignment purpose of the RICH2 sub-components.

Avoiding a large amount of light onto the HPD in a single shot requires to analyse accumulated pictures integrating on many events. The average number of hits per event has thus been set to be less than one photoelectron per HPD.

### 3.1 Reconstruction Algorithm

In this section the reconstruction algorithm [7, 16] is briefly summarised. The algorithm is made of three steps:

**Search for local maxima** The entire HPD chip is scanned, pixel by pixel, using a recursive function that looks for the absolute maximum inside a subregion surrounding the pixel. Whenever a candidate maximum is found, the search region is recentered around the candidate maximum and the search for the maximum is repeated. If a different pixel is found with a bigger number of hits, it becomes the new candidate maximum, the previous one is rejected and the procedure is repeated again.

The absolute maximum found in the subregion is rejected if its number of hits is smaller than the median value computed on the entire HPD matrix.

All the pixels labelled as candidate maxima are then excluded and the search continues in the rest of the HPD chip.

**Clustering** A recursive function looks for other local maxima in the region around the absolute maxima found at the previous step and builds the cluster.

**Estimation of the cluster center** Two different methods have been implemented and compared: the average of the position of the pixels in the cluster weighted by the number of hits and a Gaussian fit of the cluster profile. They give compatible results. In both cases the standard deviation of the reconstructed centroids is  $\lesssim 0.45$  pixel.

Two main factors can deteriorate the reconstruction procedure: noisy pixels and ion-feedback effects: they are described below.

#### 3.1.1 Noisy pixel masking

During the analysis procedure noisy pixels ( $< 1\%$  of the pixels) in the HPDs have been identified using the reconstruction algorithm so that a masking procedure has been implemented. In fact it is important to apply a procedure that can distinguish between noisy pixels and genuine local light maxima, because a noisy pixel can satisfy the conditions to be considered as a local maximum. All real local light maxima, that is local maxima corresponding to a light spot, have approximately the same number of hits, since the projected light is uniform. On the contrary noisy pixels have a number of counts that is usually larger by an order of magnitude. Therefore all local maxima with a factor of two more counts with respect to other local maxima found in the same HPD, are rejected. The different parameters were tuned so that noisy pixels are rejected without losing any real local light maximum.

#### 3.1.2 Ion-feedback reduction

Residual gas inside the HPD can cause ion-feedback [17]; consisting in a photoelectron which ionises molecules of the residual gas, creating positive ions which then drift to the photocathode.



Ions hitting the photocathode produce secondary electron emission. A ion-feedback event is characterised by a large number of hits grouped in clusters in the HPD centre.

For the majority of the HPDs this effect only gives a small noise increase. However for 10% – 20% of the HPDs the ion-feedback rate can be so high that it spoils the signal and provokes accelerated ageing of the photocathode and a decrease of the detection efficiency.

If the ion-feedback background is large, the algorithm may have problems to reconstruct the light spot positions.

A study to reduce this background has been performed analysing the behaviour of two variables: the number of hits per event and the maximum cluster size per event. Comparing HPDs with large ion-feedback to HPDs without it, one can define selection cuts to reject ion-feedback events. A cut on the number of hits larger than three and on the cluster size larger than two has been chosen (see Figure 5). The performance of the algorithm is shown in Figure 6 for one single HPD affected by ion-feedback. The drop of the signal efficiency due to these cuts is negligible ( $< 2\%$ ).

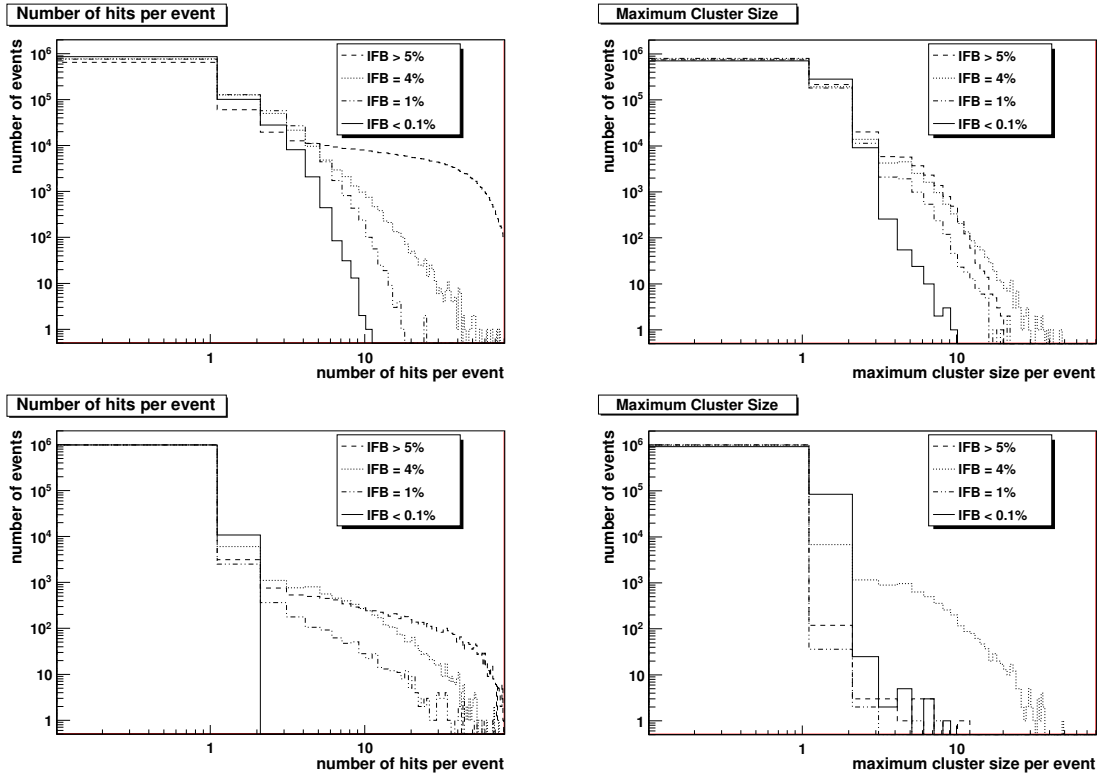


**Figure 5.** Histogram of the number of hits and maximum cluster size, used to characterise the ion-feedback effect in data with the light pattern (top) and dark count data (bottom).

After removing the noisy pixels and the effects of ion-feedback it is possible to reconstruct the spots projected by the light projector as shown in Figure 7.

#### 4. Correction of the Magnetic Distortions

Different data sets have been taken with the LHCb magnet on and off, at full and half-field and

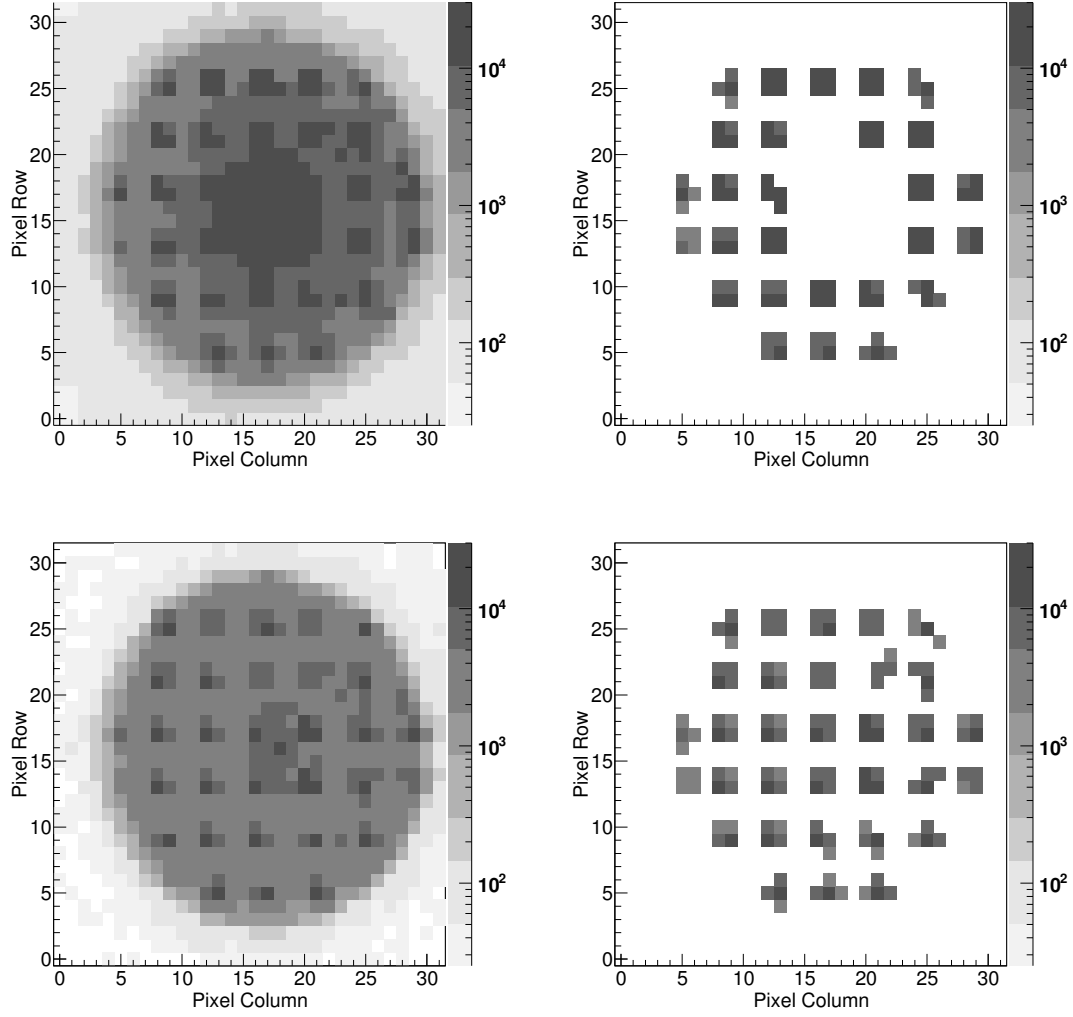


**Figure 6.** Hit Map for one single HPD before (top figures) and after the ion-feedback cuts (bottom figures). In the two top figures the algorithm is not able to reconstruct clusters due to the ion-feedback effect. After applying the cuts the ion-feedback is reduced and the light spots are reconstructed correctly as shown in the bottom figures.

with both magnet polarities.

A distortion effect is clearly visible in some of the HPDs. As the stray magnetic field is not uniform in the HPD matrix, the size of the effect depends on the position of each tube inside the matrix. Two examples are shown in Figure 8.

#### 4.1 Parametrisation

The expected image distortion in RICH2 is a non-uniform rotation and stretch of the light spots with respect to the HPD centre, while translations are expected to be negligible. This means that the stray magnetic field has a non-negligible component along the HPD geometrical axis, while the component perpendicular to it is small, in agreement with simulation results [11].

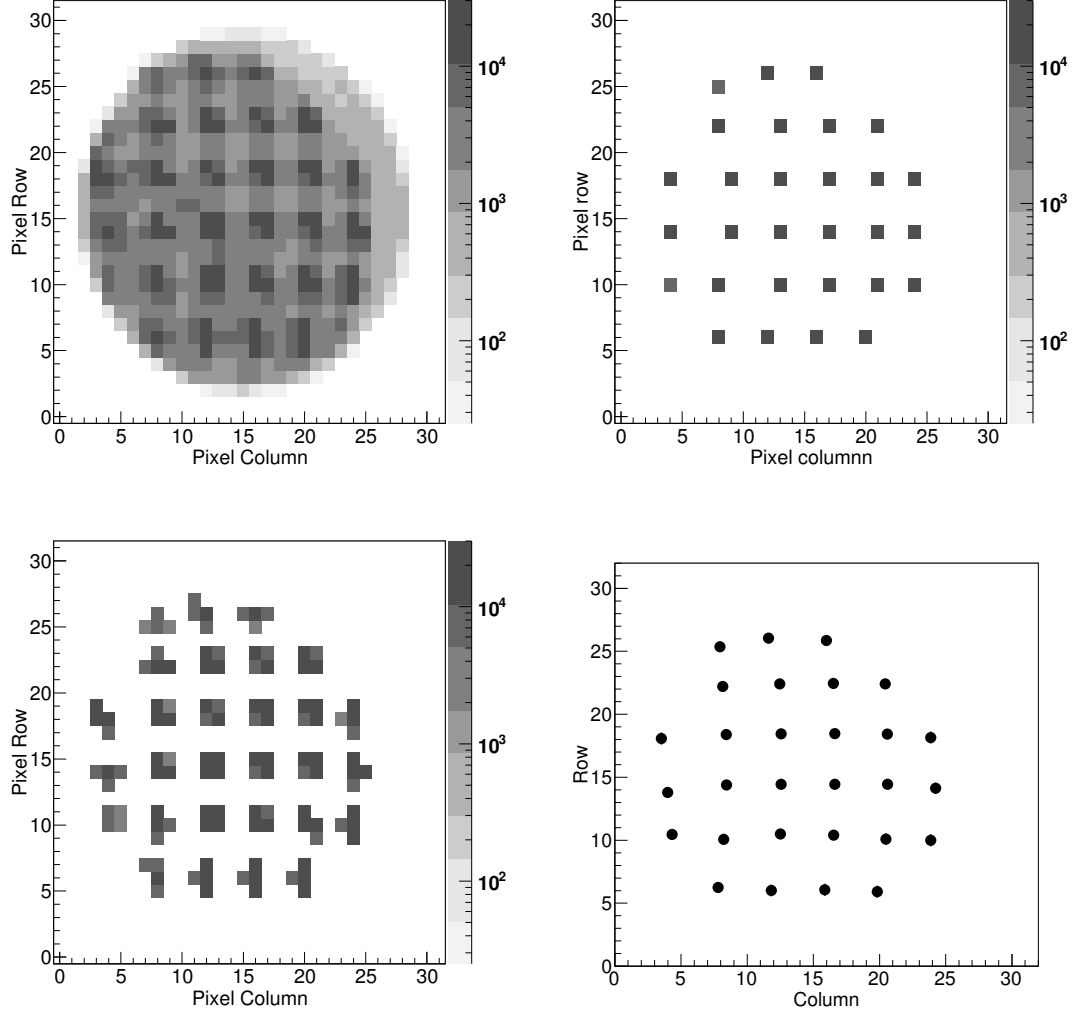


**Figure 7.** Light spot position reconstruction procedure: raw data (top left), local reference maxima (top right), clusters (bottom left) and cluster centres (bottom right).

The distortion can be parametrised by a function of the light spots position with respect to the HPD centre, expressed in polar coordinates  $(r, \theta)$ :

$$\vec{d}_{i,j}(r, \theta) = \Delta\theta_{i,j}(r, \theta) \vec{e}_\theta + \Delta r_{i,j}(r, \theta) \vec{e}_r \quad (4.1)$$

where  $i$  denotes the HPD and  $j$  denotes the light spot inside it.

The average rotation angle for each HPD is given by

$$\langle \Delta\theta \rangle_i = \frac{\sum_{j=0}^{n_i} \Delta\theta_{i,j}}{n_i}, \quad (4.2)$$

where  $n_i$  is the number of light spots reconstructed in the HPD  $i$ ,  $\Delta\theta_{i,j}$  is the rotation angle of the reconstructed light spot  $j$  with magnetic field on with respect to its position with magnetic field off and calculated with respect to the centre of the HPD  $i$ .

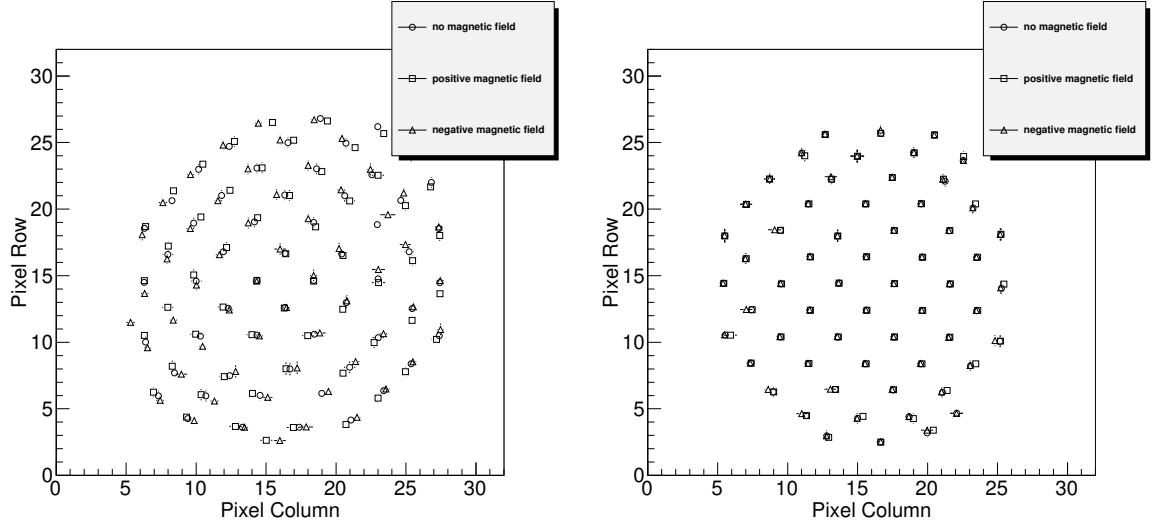


**Figure 8.** Reconstructed cluster centres for two different HPDs located in two different positions inside the HPD matrix : square and triangle markers for magnetic field on (opposite polarities); circle marker for magnetic field off.

The average rotation angle is related to the average magnetic field  $\langle B \rangle_i$  at the location of the tube. If the magnetic field is small and uniform inside the HPD volume, one can assume that the rotation angle is, to a first approximation, proportional to the average magnetic field:

$$\langle \Delta\theta \rangle_i \propto \langle B \rangle_i. \quad (4.3)$$

The sign of the rotation angle is related to the direction of the magnetic field. The effective magnetic field map inside the HPD volume, estimated from the average image rotation angle, is shown in Figure 9. The rotation angle changes its sign when going from the top to the bottom region of the HPD matrix and it is close to zero in the central region. The rotation effect  $\langle \Delta\theta \rangle \lesssim 0.1$  rad, is clearly detectable and measurable. Its value is not exactly symmetrical along the vertical direction since the HPD matrix is not symmetrically located inside the overall shielding box.

A modulation as a function of the HPD columns is also clearly visible (see Figure 10): the first and the last column of each side show a smaller rotation angle with respect to the central columns. This is consistent with the fact that the lateral columns, being closer to the vertical walls of the overall shielding are affected by a smaller magnetic field than the central columns. The effect of the overall shielding box is also evident for the HPDs installed on top or bottom of each column. All these effects are compatible with the results from simulations.

Since the magnetic field intensity is different for each HPD, the distortion parameters are different from HPD to HPD. However, after normalising the parameters to the average rotation angle, which is proportional to the strength of the magnetic field, one can find universal parameters for all HPDs.

Two curves are needed to parametrise the distortion effect (see Figure 11): the rotation angle

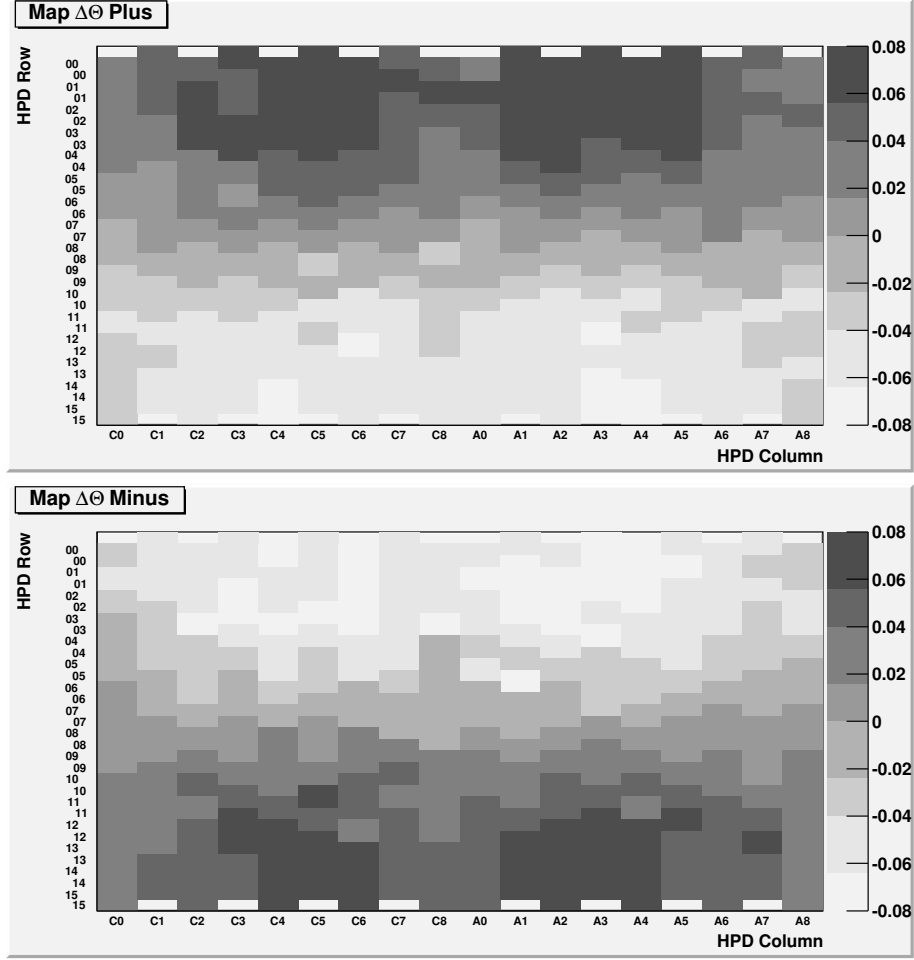


**Figure 9.** Effective magnetic field map inside the HPD enclosure, determined from the average image rotation angle for each HPD. Column and row numbers of the HPD position inside the matrix are given. The HPDs in the matrix are positioned in an hexagonal close pack arrangement. The double numbers in the vertical axis refer to even and odd columns that are vertically staggered.

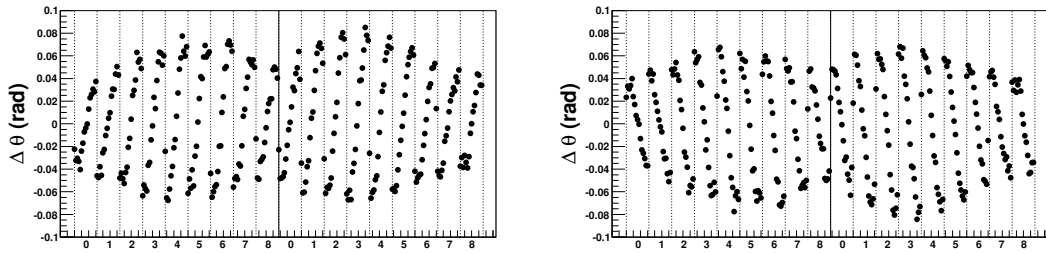


**Figure 10.** HPD average image rotation angle for the two HPD matrices for positive magnetic field (left) and negative magnetic field (right). The numbers on the axis indicate the column number of the matrix. The change of the magnetic field along each HPD column is clearly visible as well as the fact that the magnetic field is stronger in the central region.

and the radius variation of each single spot of the pattern:

$$\begin{cases} \Delta\theta_{i,j} = \langle\Delta\theta\rangle_i f_\theta(r_{i,j}) \\ \Delta r_{i,j} = \langle\Delta r\rangle_i f_r(r_{i,j}) \end{cases} \quad (4.4)$$

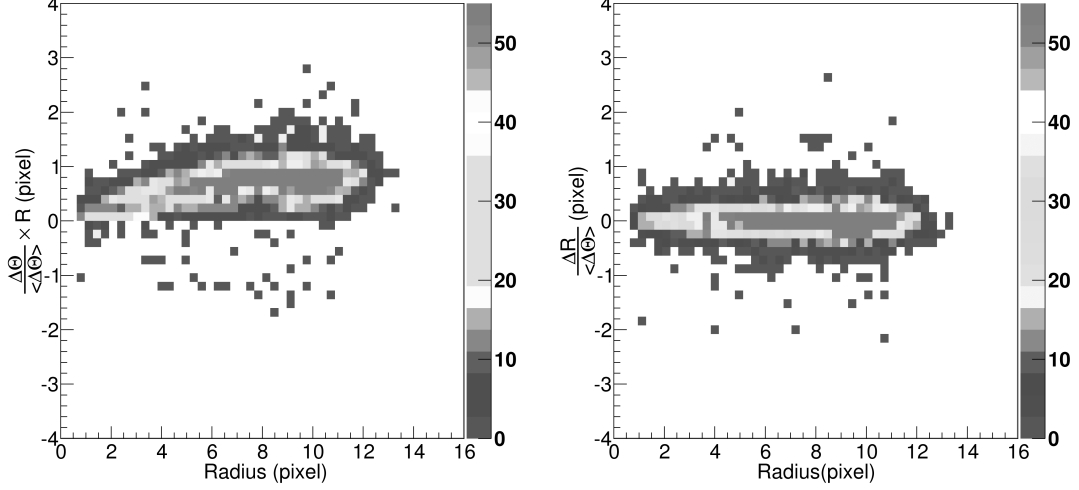


**Figure 11.** Rotation angle (left) and radius variation (right) of the light spots as a function of the distance from the HPD centre.

In Figure 11 the quantity  $r_{i,j} \Delta\theta_{i,j}$  was used instead of  $\Delta\theta_{i,j}$  since for small  $r$  the error on the light spot angle is large, as distances are measured, not angles.

From the first plot in Figure 11 one can see that the quantity  $r\Delta\theta$  increases as a function of the radius up to  $r \sim 6$  pixel and then it becomes approximately constant. From the second plot in Figure 11 one can assume that, on average, there is no significant change of the light spots distance from the centre.

Therefore there is only a non-uniform rotation and no stretch of the image within the current sensitivity.

In order to parametrise the angular distortion a fit with a second order polynomial function has been performed:

$$f_\theta(r) = ar + br^2 \quad (4.5)$$

obtaining:

$$a = 0.17 \pm 0.04 \text{ pixel}^{-1} \quad b = -0.009 \pm 0.004 \text{ pixel}^{-2} \quad (4.6)$$

Therefore the magnetic distortion effects can be corrected applying to all HPDs using the universal relations

$$\begin{cases} \Delta\theta_{i,j} = \langle\Delta\theta\rangle_i f_\theta(r_{i,j})/r_{i,j} \\ \Delta r_{i,j} = 0 \end{cases} \quad (4.7)$$

with the same parameters regardless of their position. Moreover the same parameters are valid, with a sign inversion, for the two opposite polarities of the magnetic field.

Measurements were also taken at half-nominal field values, demonstrating that the rotation angle is proportional to the magnetic field intensity.

#### 4.2 Correction procedure

Once the magnetic distortion effect has been parametrised, it is possible to correct the data. The corrections have been applied to the light spot positions with magnetic field on and then compared to the positions with magnetic field off. The inverse coordinate transformations from the non-corrected coordinates,  $(x_0^{(nc)}, y_0^{(nc)})$ , to the corrected ones,  $(x^{(c)}, y^{(c)})$ , via  $\Delta\theta_{i,j}$ , are:

$$\begin{cases} x^{(c)} = x_0^{(nc)} \cos(-\Delta\theta) - y_0^{(nc)} \sin(-\Delta\theta) \\ y^{(c)} = x_0^{(nc)} \sin(-\Delta\theta) + y_0^{(nc)} \cos(-\Delta\theta) \end{cases} \quad (4.8)$$

where the indices  $i$  and  $j$  have been suppressed for clarity.

The resolution obtained after the correction procedure (see the two left plots of Figure 12), amounts to

$$\sigma_x \simeq 0.18 \text{ pixel} \quad \sigma_y \simeq 0.18 \text{ pixel} \quad (4.9)$$

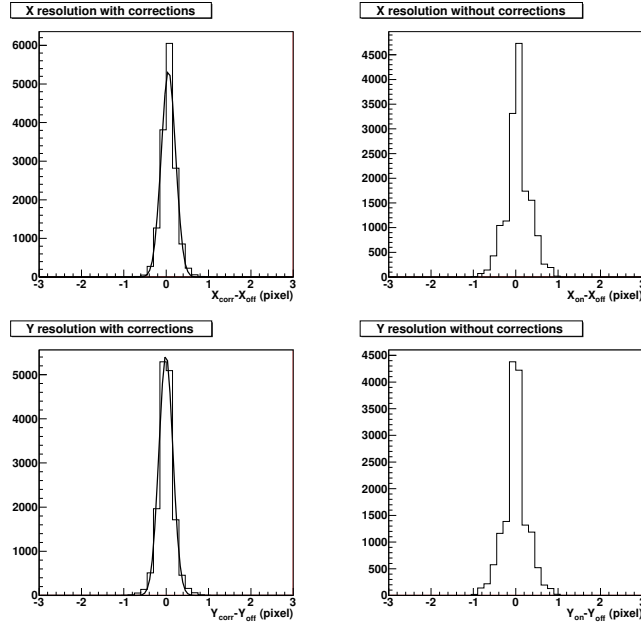


**Figure 12.** Resolution, in the  $x$  and  $y$  coordinates, with (left) and without (right) applying the correction procedure (in pixels).

This resolution must be compared to the one found without any correction of the magnetic field effects, (see the two right plots of Figure 12), that is:

$$\text{RMS}_x \simeq \text{RMS}_y \simeq 0.33 \text{ pixel} \quad (4.10)$$

For the sake of comparison the resolution due to the finite pixel size is  $\sigma \simeq 0.29 \text{ pixel}$ . The correction procedure therefore restores the optimal resolution of the Cherenkov angle [7].

## 5. Correction of the magnetic distortion in the first LHCb data

The correction parameters, determined as described before, are stored in the LHCb condition database and were used on the first data taken by LHCb in 2010.

Saturated Cherenkov rings were reconstructed in minimum bias data, taken with magnetic field on and with both polarities.

The rings were reconstructed with and without applying the magnetic field distortion correction. The measured Cherenkov angle distribution of saturated Cherenkov rings was fitted with a Gaussian plus a second-order polynomial. The standard deviation of the Gaussian fit is summarised in Table 2. As the residual stray magnetic field is small in the central region of the HPD matrix, the data in Table 2 show that the correction has little effect in that region. On the other hand the residual stray magnetic field is not negligibly small in the external regions of the HPD matrix, where the correction improves the resolution.

The correction parameters restore the optimal shape of the ring that otherwise would be distorted. This decreases the standard deviation of the measured Cherenkov angle distribution improving the capability of the PID system.

**Table 2.** Standard deviation of the Gaussian plus second order polynomial fit of saturated Cherenkov rings without and with magnetic distortion corrections.

<b>Magnetic field down</b>		
	external	central
Without correction	0.81 mrad	0.73 mrad
With correction	0.76 mrad	0.73 mrad
<b>Magnetic field up</b>		
	external	central
Without correction	0.76 mrad	0.70 mrad
With correction	0.73 mrad	0.70 mrad

## 6. Conclusions

A system to measure the effects of the magnetic distortions in the RICH2 detector of LHCb has been set up.

The residual stray magnetic field, that has a predominant component parallel to the HPD geometrical axis, causes a small rotation of the photoelectrons from the nominal trajectory given by the HPD electrostatic field.

By applying the correction procedure described in this note the resolution improves from  $\sim 0.33$  pixel to  $\sim 0.18$  pixel.

The effect of the correction has been cross-checked on real data. It improves the Cherenkov angle resolution especially in the external region of the HPD matrix. The optimal particle identification capability of RICH2 is restored.

It is planned to repeat the projector measurements during each shut-down periods to check the stability of the parameters and look for possible hysteresis effects.



## 7. Acknowledgements

We thank the technical and administrative staff at CERN and at the LHCb institutes, and acknowledge support from the National Agencies, in particular CERN and INFN (Italy). We also thank C. Matteuzzi and O. Ullaland for many useful discussions and support.

## References

- [1] LHCb Collaboration, *The LHCb Detector at the LHC*, 2008 *JINST* **3** S08005.
- [2] S. Myers, *LHC Commissioning And First Operation*, in *Proceedings of 1<sup>st</sup> International Particle Accelerator Conference: IPAC'10, Kyoto, Japan, (2010)*, <http://accelconf.web.cern.ch/AccelConf/IPAC10>.
- [3] The LHCb Collaboration, *Roadmap for selected key measurements of LHCb*, LHCb-PUB-2009-029 (2010), [arXiv:0912.4179].
- [4] C. D'Ambrosio, *Commissioning of the LHCb RICH detectors*, *Nucl. Instr. and Meth. A* **595** (2008) 36
- [5] T. Gys, *The pixel hybrid photon detectors for the LHCb-rich project*, *Nucl. Instrum. Meth. A* **465** (2001) 240; C. D'Ambrosio and H. Leutz, *Hybrid photon detectors*, *Nucl. Instrum. Meth. A* **501** (2003) 463; M. Moritz et al., *Performance study of new pixel hybrid photon detector prototypes for the LHCb RICH counters*, *IEEE Trans. Nucl. Sci.* **51**, **3** (2004) 1060; S. Eisenhardt, *Production and tests of Hybrid Photon Detectors for the LHCb RICH detectors*, *Nucl. Instr. and Meth. A* **595** (2008) 142; and references therein.
- [6] C. Frei, *Position of the HPDs in the RICH2 detector*, EDMS document, <https://edms.cern.ch/document/965834>.
- [7] R. Cardinale, *Identificazione di particelle e studio del decadimento  $B^\pm \rightarrow K^\pm \pi^0$  con il rivelatore RICH di LHCb*, CERN-THESIS-209-167 (in italian), <http://cdsweb.cern.ch/record/1309247>.
- [8] F. Xing, *Magnetic distortion calibration for LHCb RICH detectors*, *Nucl. Instrum. Meth. A* In Press, Corrected Proof (2010).
- [9] G. Aglieri Rinella et al., *Performance Studies of Pixel Hybrid Photon Detectors for the LHCb RICH Counters*, *Nucl. Phys. Proc. Suppl.* **150** (2006) 285.
- [10] M. Losasso, *Magnetic field of the LHCb dipole magnet at sub-detectors, cryoplant and electronic racks*, Note LHCb-2000-084, <http://cdsweb.cern.ch/record/681341>
- [11] T. Gys, *Magnetic field simulations for the LHCb-RICH 2 detector*, Note LHCb-2002-029, <http://cdsweb.cern.ch/record/681217> and references therein.
- [12] G. Aglieri Rinella et al., *Characterisation and compensation of magnetic distortions for the pixel Hybrid Photo-Detectors of the LHCb RICH*, *Nucl. Instrum. Meth. A* **553** (2005) 120.
- [13] Technical documentation on the Samsung SP-P310ME can be found at Samsung website.
- [14] Technical documentation on the Hamamatsu H3164-10 PMTs can be found at Hamamatsu website.
- [15] M. Villa, *The LHCb RICH PMTs Readout Electronics and the Monitoring of the HPDs Quantum Efficiency*, CERN-THESIS-2007-079, <http://cdsweb.cern.ch/record/1073941>.
- [16] B. Storaci, *The LHCb RICH : its application to the study of the  $B_s \rightarrow J/\Psi$  decay channel and magnetic distortions corrections*, CERN-THESIS-2007-071, <http://cdsweb.cern.ch/record/1064967>.
- [17] S. Eisenhardt, *Hybrid Photon Detectors and Ion Feedback*, *Nucl. Instr. and Meth. A* **617** (2010) 391.